Temperature Rise and SAR Distribution at Wide Range of Frequencies in a Human Head due to an Antenna Radiation

Fatih Kaburcuk [1] and Atef Z. Elsherbeni [2]

[1] Electrical and Electronic Engineering Department
Erzurum Technical University, Erzurum, 25700, Turkey
fkaburcu@syr.edu – fatih.kaburcuk@erzurum.edu.tr

[2] Electrical Engineering Department
Colorado School of Mines, Golden, CO, 80401, USA
aelsherb@mines.edu

Abstract ─ Temperature rise and specific absorption rate distribution in a human head due to electromagnetic energy produced by an adjacent antenna are evaluated. An algorithm proposed in this paper provides these distributions at multiple frequencies using a single simulation. The head tissue parameters are used from the available three-term Debye coefficients obtained by the experimental data from 500 MHz to 20 GHz. The proposed algorithm is developed by integrating the Debye model of human head tissues parameters into the finite-difference time-domain method by using the auxiliary differential equation approach along with the use of bioheat equation for specific absorption rate and temperature computations.

Index Terms ─ Dispersive material, FDTD method, Specific Absorption Rate (SAR), temperature rise.

I. INTRODUCTION

Many researchers have studied the temperature rise and specific absorption rate (SAR) distribution in the human head due to electromagnetic (EM) radiation produced by cellular phones with different types of antennas [1–8] using the nondispersive algorithm based on the finite-difference time-domain (FDTD) method. In the previous work [1–8], the SAR computation for a human head was conducted at only one frequency of interest using a single simulation because of the depressiveness properties of the biological tissue. Therefore, the thermal analysis and SAR computation for multiple frequencies was not integrated into the nondispersive algorithm because the EM properties of the biological tissues are dependent on frequency.

In this paper, a dispersive algorithm is developed to obtain SAR and temperature distributions at multiple frequencies of interest from a single FDTD simulation. The dispersive algorithm is based on the integration of Debye tissue model into the FDTD method using the ADE as presented in [9] along with the Pennes bioheat equation from [10]. The dispersive EM properties of the human head tissues for a wide range of frequencies (500 MHz to 20 GHz) used in this investigation are based on the three-term Debye coefficients (the relative permittivity of medium at infinite frequencies, the static relative permittivity, and the relaxation time) calculated and tabulated in [11]. The dispersive algorithm provides the temperature rise and SAR distribution in the head at multiple frequencies of interest in a single FDTD simulation.

The simulation procedure of the dispersive algorithm can be achieved in the following steps: 1) EM simulation of the dispersive head model using the FDTD method due to a multi-frequency source; 2) computation of the steady-state SAR distribution due to the EM simulation at the frequencies of interest; 3) computation of the steady-state temperature distribution using the bioheat equation when SAR=0; and 4) computation of the final temperature distributions at the frequencies of interest by substituting the steady-state SAR distribution in the bioheat equation. Finally, the difference of the final and steady-state temperature distributions in the head gives the temperature rise distribution. As expected, the computed temperature rise and SAR in the head are found to be different for different frequencies because of the frequency dependent of the biological tissues EM parameters. The temperature rise in the head due to the antenna is insufficient to cause a remarkable change on EM parameters of head tissues.

To prove the validity of the developed algorithm, the radiation from an antenna is evaluated in the presence of a heterogeneous head model obtained from [12]. The temperature rise and SAR distributions in the head at multiple frequencies centered around 900 MHz and 1.5 GHz are obtained using multiple simulations using the traditional nondispersive algorithm as well as using a single FDTD simulation based on the developed

Submitted On: October 18, 2017
Accepted On: January 22, 2018

algorithm. Furthermore, in order to show the effect of distance between the head model and the antenna, the maximum temperature rise and SAR in the head are calculated for a set of separation distances. This work will facilitate the future interaction between a human head and EM plane waves produced by 5G base stations.

II. MODEL AND METHODS

A. Human head model

The realistic and heterogeneous head model used in this work has been constructed from a ZUBAL MRI head phantom [12]. MATLAB is used to read and resampled the head data which consists of 8 tissues, including skin, muscle, bone, blood, fat, lens, and white and grey matter. The head model consists of 86(width)×110(depth)×120(height) cubic cells. In order to ensure the numerical stability in the FDTD method, a cell dimension should be less than $\lambda_{\min}/10$, where $\lambda_{\min}$ is the wavelength of the highest frequency in free space. The cell size used here is 2 mm in the three Cartesian directions. The time step is restricted by the Courant stability criterion.

B. Dispersive head tissues

The head model used in this paper consists of eight dispersive tissues. A numerical procedure developed in [11] provides two-term and three-term Debye coefficients to accurately fit the experimental data from [13] for the head tissues for the frequency range 500 MHz to 20 GHz. The three-term Debye coefficients of the head tissues used in this work are given in Table 1. The complex relative permittivity $\left(\varepsilon_r^*(\omega)\right)$ for three-term Debye coefficients is given [11] as:

$$\varepsilon_r^*(\omega) = \varepsilon_\infty + \sum_{k=1}^{3} \frac{\Delta\varepsilon_k}{1 + j\omega\tau_k}, \tag{1}$$

where ε_∞ is the relative permittivity at infinite frequencies, ε_k and τ_k are the static relative permittivity and the relaxation time of the kth term, respectively.

Table 1: Three-term Debye parameters of head tissues for the frequency range 500 MHz to 20 GHz

Tissue	ε_∞	$\Delta\varepsilon_1$	$\Delta\varepsilon_2$	$\Delta\varepsilon_3$	τ_1[ps]	τ_2[ps]	τ_3[ps]
Skin	4.136	32.51	2.499	125.6	7.248	527.2	1.380
Fat	2.994	2.467	6.066	31.39	3.970	7904	3.739
Bone	3.532	4.992	12.47	34.85	5.811	133.5	1.172
Blood	5.939	46.72	8.064	693.1	7.203	125.2	4.387
Muscle	5.896	45.70	2.956	324.1	6.474	139.0	3.443
Lens	5.415	32.56	8.388	304.1	6.719	106.3	3.909
W. Matter	5.338	30.04	2.090	70.50	7.181	225.7	1.156
G. Matter	5.380	42.16	2.754	137.1	7.187	224.6	1.399

C. FDTD method and antenna

The proposed dispersive algorithm and the nondispersive algorithm are used to analyze the interactions between the human head model and an antenna as a wave source. The antenna is placed 24 mm away from the right ear of the head model and excited by a voltage source with a Gaussian waveform containing the frequencies of interest. The width and time delay of the Gaussian waveform are set to T=50 ps and 4.5T, respectively [9]. In this work, CPML [14] absorbing boundaries are applied at the borders to truncate the problem domain.

D. SAR calculation in the head

The FDTD method is used for the computation of the SAR which is used in the temperature rise calculation. The average electric (E) field components at the center of each cell for all frequencies of interest are determined by using the discrete Fourier transform during the FDTD time-marching loop. Once the FDTD time-marching loop is completed, the amplitudes of the E field components are used for the calculation of the steady-state SAR distribution at each frequency of interest. The calculated steady-state SAR at each frequency of interest is considered the EM heat source and is used in the temperature rise calculation of the head. The SAR is defined at a given location as:

$$SAR(i,j,k) = \frac{\sigma(i,j,k)}{2\rho(i,j,k)}\left(\left|E_x(i,j,k)\right|^2 + \left|E_y(i,j,k)\right|^2 + \left|E_z(i,j,k)\right|^2\right), \tag{2}$$

where $\sigma(i,j,k)$ and $\rho(i,j,k)$ are the electric conductivity and mass density [kg/m^3] of the tissue at a given location, respectively. In Equation (2), an averaging of E_x, E_y, and E_z is performed to obtain the corresponding values at the exact location of interest. The computed SAR distribution is normalized to the antenna output power. For calculating the peak SAR over 1 gram of tissue in the head, the IEEE standard C95.3-2002 is considered [15].

E. Temperature rise calculation in the head

When the steady-state SAR distribution in the head is computed, the thermal simulation is performed by solving the bioheat equation [10] which consists of two simulations: In the first simulation, the temperature distribution in the head is calculated by using the bioheat equation without EM power (i.e., SAR=0) during the thermal time-marching loop. This calculation is carried out until the convergence is reached. The calculated temperature distribution is considered as the steady-state temperature distribution in the head. In the second simulation, the final temperature distribution is calculated by substituting the obtained steady-state SAR distribution into the bioheat equation. The temperature rise distribution is achieved by taking the difference between final and steady-state temperature distributions.

The bioheat equation is given by:

$$\rho \cdot C \cdot \frac{\partial T}{\partial t} = K \cdot \nabla^2 T + \rho \cdot SAR - B \cdot \left(T - T_b\right), \tag{3}$$

where T is the temperature of the tissue at time t, ρ is the mass density of the tissue [kg/m^3], C is the heat capacity

of the tissue [J/(kg·°C)], K is the thermal conductivity of a tissue [J/(m·°C)], B is the blood perfusion rate [W/(m^3.°C)], and T_b is the blood temperature.

Heat exchange [1] between the skin surface and air is modeled by imposing the continuity of the heat flow perpendicular to skin surface as a boundary condition. The boundary condition applied to skin surface and also internal cavity surface of the head is expressed as:

$$K \cdot \frac{\partial T}{\partial n} = -h \cdot \left(T - T_a\right), \tag{4}$$

where T_a is the air temperature, n is the unit normal vector to the skin surface or internal cavity, and h is the convection heat transfer coefficient [W/(m^2·°C)].

During each thermal time-step, the bioheat equation in (3) is applied to all tissues in the head and then the boundary condition in (4) is applied to the skin surface and internal cavity surface of the head. The temperature is computed at the center of each cell with a spatial step d equal to that used in the FDTD simulation and a thermal time-step equal to Δt. The discretized form of the bioheat equation in (3) and the boundary condition in (4) at mth thermal time-step with a cell indexed as (i, j, k) can be written, respectively in (5) and (6) as:

$$T^{m+1}(i,j,k) = \left(\begin{array}{c} T^m(i,j,k) + \frac{\Delta t}{C(i,j,k)} \cdot SAR(i,j,k) \\ - \frac{\Delta t}{\rho(i,j,k) \cdot C(i,j,k)} \cdot B(i,j,k) \cdot \left[T^m(i,j,k) - T_b \right] \\ + \frac{\Delta t}{\rho(i,j,k) \cdot C(i,j,k) \cdot d^2} \cdot K(i,j,k) \cdot \\ \left[\begin{array}{c} T^m(i+1,j,k) + T^m(i,j+1,k) \\ + T^m(i,j,k+1) + T^m(i-1,j,k) \\ + T^m(i,j-1,k) + T^m(i,j,k-1) - 6T^m(i,j,k) \end{array} \right] \end{array} \right), \tag{5}$$

$$T^{m+1}\left(i,j,k_{\min}\right) = \frac{K \cdot T^m\left(i,j,k_{\min}+1\right)}{K + h \cdot d} + \frac{T_a \cdot h \cdot d}{K + h \cdot d}. \tag{6}$$

The finite-difference approximation of the boundary condition in (6) computed at the skin/air interface is given only for the z-direction, which is normal to the skin surface of the head. Similarly, this approximation can be applied to x- and y-directions which are normal to the skin surface of the head. The convection heat transfer coefficients (h) is set to 10.5 [W/(m^2·°C)] from the skin surface to air and 50 [W/(m^2·°C)] from the internal surface to the internal cavity [1]. Table 2 gives the mass density (ρ) and thermal parameters (C, K, B) of the head tissues [2, 5, 7]. The air temperature (T_a) and initial head temperature (T_b) in the simulations were set to 20 °C and 37 °C, respectively. In order to avoid the numerical instability, the thermal time-step (Δt) is chosen to satisfy the following criterion [1]:

$$\Delta t \le \frac{2\rho C d^2}{12K + Bd^2}. \tag{7}$$

III. NUMERICAL RESULTS

In the first part of this section, the temperature rise and SAR distributions are obtained using the proposed dispersive algorithm at all frequencies of interest in a single simulation. In the second part, these distributions are obtained using the nondispersive algorithm by performing multiple simulations, each at a single frequency. These two approaches were conducted to compare results and to show the performance and efficiency of the developed dispersive algorithm. Finally, in the last part of this section, the performance of the developed algorithm and the effect of distance from the head model to the antenna on the SAR and temperature rise are presented. In all simulations, the output power of the antenna was set to 0.6 W for 900 MHz and 0.27 W for 1.5 GHz as in [1].

Table 2: Mass density and thermal parameters of the head tissues

Type of Tissue	ρ [kg/m^3]	C [J/(kg.°C)]	K [W/(m.°C)]	B [W/(m^3.°C)]
Skin	1125	3600	0.42	9100
Fat	916	3000	0.25	1700
Bone	1810	1300	0.40	1000
Blood	1058	3900	0.56	0
Muscle	1047	3800	0.50	2700
Lens	1100	3000	0.40	0
W. Matter	1038	3500	0.50	40000
G. Matter	1038	3800	0.57	40000
Air (internal)	1.2	1000	0.03	0

A. Temperature rise and SAR distributions in the head using the proposed dispersive algorithm

In order to provide solutions at multiple frequencies, an antenna with at least two frequency bands is required to radiate towards the head. Thus, a modified dipole antenna of 156 mm length and 0.74 mm diameter is modified by adding two passive wires replaced at a distance of 4 mm at the two sides of a dipole antenna as shown in Fig. 1. The diameter and length of the passive wires are 1.56 mm and 88 mm, respectively. The center operating frequencies of this loaded dipole antenna are 900 MHz and 1.5 GHz. The input reflection coefficient (S_{11}) and directivity pattern in the xy plane cut at 900 MHz and 1.5 GHz are shown in Fig. 2.

The temperature rise and SAR distributions of the head due to the antenna are calculated at three frequencies centered at 900 MHz and at three other frequencies centered at 1.5 GHz using a single simulation. The maximum 1 gram averaged SAR value in the head is 1.628 Watt/kg at 900 MHz and 1.068 Watt/kg at 1.5 GHz. The SAR values calculated in this work are found to be exactly the same as those values reported in [1]. Figure 3 shows the 1 gram averaged SAR distribution at 900 MHz and 1.5 GHz in the x-y cross section of the head model. Figure 4 shows the resulting temperature rise distribution at 900 MHz and 1.5 GHz in the x-y cross section of the head model. The maximum temperature rise in the head is 0.281 °C at 900 MHz and 0.149 °C at

1.5 GHz. The maximum temperature rise calculated in [1] is 0.18 ºC at 900 MHz and 0.15 ºC at 1.5 GHz. There is some small difference between our results and those published in [1], mainly due to the fact that the head model used in this paper is different and the head phone set as a source in [1] is different from the dipole antenna used in this paper. The maximum temperature variation in the head as a function of time is shown in Fig. 7 at 870, 900, 930 MHz and 1.46, 1.50, 1.54 GHz. It can be seen from Fig. 5 that the temperature increases rapidly over the first 10 minutes, then temperature increase slows down, and the maximum (steady-state) temperature is reached after 32 minutes of exposure.

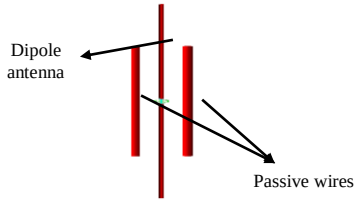

Fig. 1. The dipole antenna loaded with two passive wires.

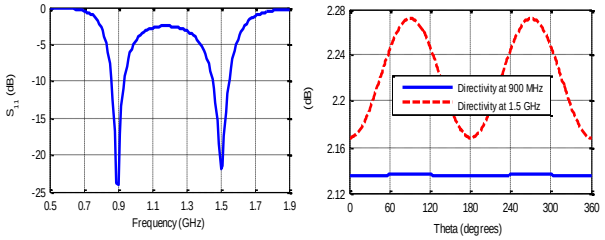

Fig. 2. S_{11} and directivity pattern in the *xy* plane cut.

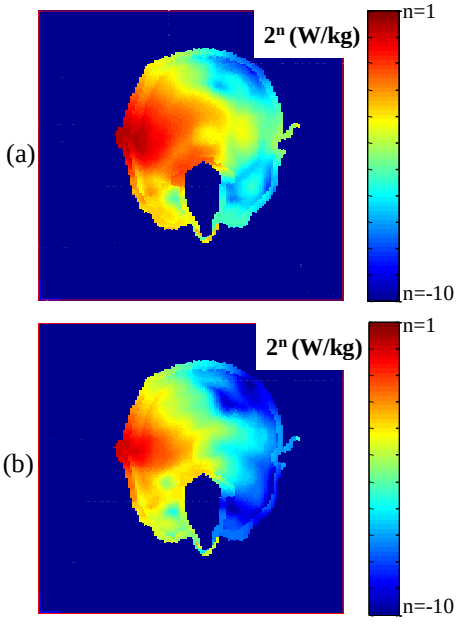

Fig. 3. 1 gram averaged SAR distribution in the head at (a) 900 MHz and (b) 1.5 GHz.

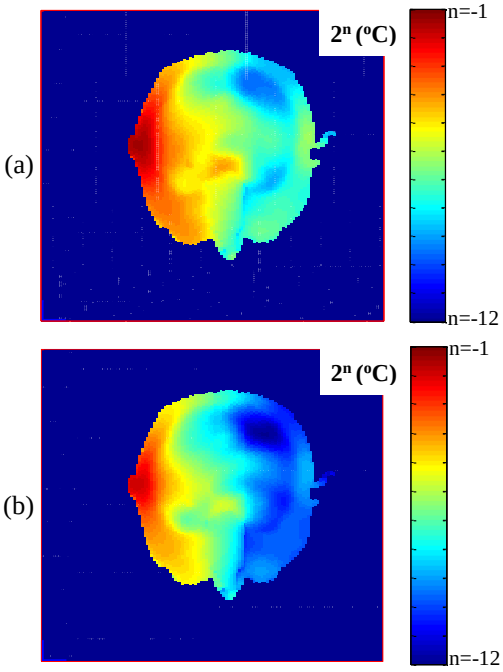

Fig. 4. Temperature rise distribution in the head at (a) 900 MHz and (b) 1.5 GHz.

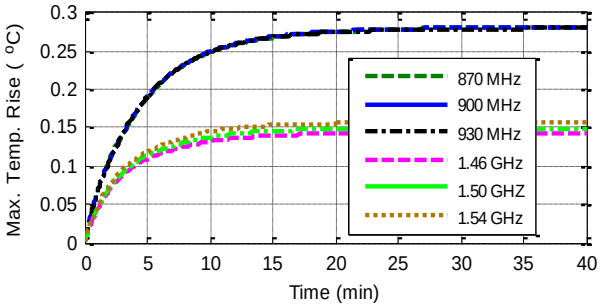

Fig. 5. Maximum temperature rise in the head vs. time at 870, 900, 930 MHz and 1.46, 1.50, 1.54 GHz.

B. Temperature rise and SAR distributions in the head using the nondispersive algorithm

In order to prove the validity of the proposed dispersive algorithm, the temperature rise and SAR distributions in the head are calculated at the same frequencies listed in the above section, but using multiple simulations using the nondispersive algorithm. The SAR and temperature rise distributions obtained from these simulations agree very well with the results obtained from the single simulation shown in previous section. The 1 gram averaged SAR and temperature rise distributions are shown in Fig. 6 and Fig. 7, respectively. The maximum 1 gram averaged SAR value in the head is 1.628 Watt/kg at 900 MHz and 1.068 Watt/kg at 1.5 GHz. The maximum temperature rise in the head is 0.281 ºC at 900 MHz and 0.149 ºC at 1.5 GHz.

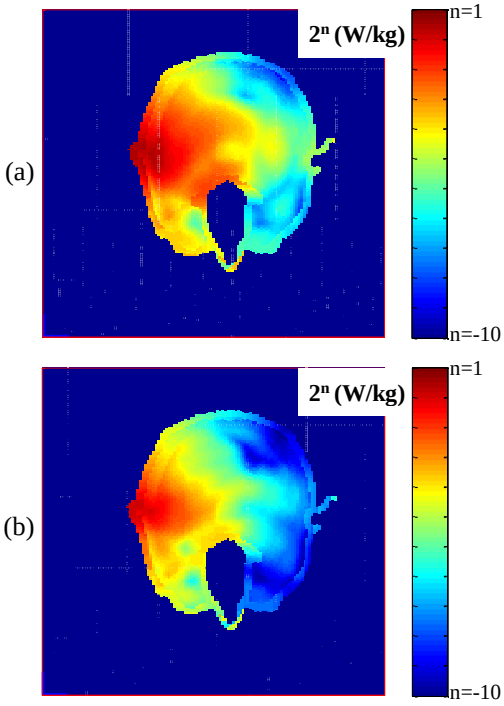

Fig. 6. 1 gram averaged SAR distribution in the head at (a) 900 MHz and (b) 1.5 GHz.

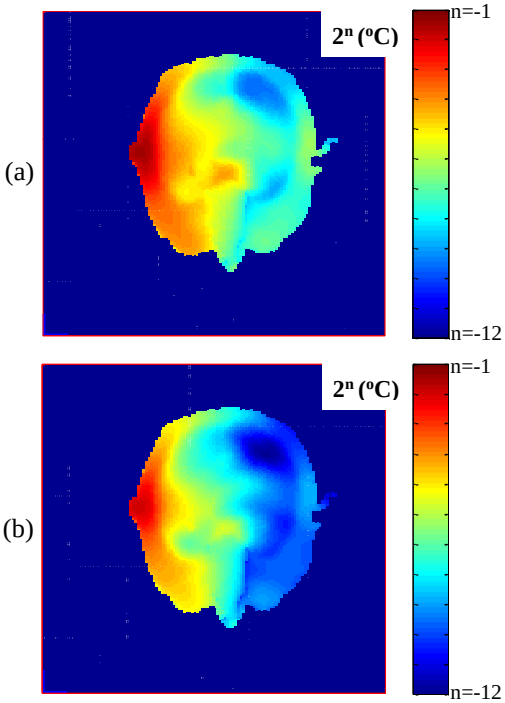

Fig. 7. Temperature rise distribution in the head at (a) 900 MHz and (b) 1.5 GHz.

C. Performance of the dispersive algorithm

For practical applications, it is always necessary to expect results at multiple frequencies. The formulation of the dispersive algorithm [9] is more complicated than that of the nondispersive algorithm. However, the dispersive algorithm can provide solutions at multiple frequencies using a single simulation, whereas the nondispersive algorithm can also provide solutions at multiple frequencies but using multiple simulations. To show the efficiency of the proposed dispersive algorithm, the computation time of both algorithms is recorded for results at six frequencies and are shown in Fig. 8. As shown, when the number of frequencies of interest is increased the dispersive algorithm is more efficient than the nondispersive algorithm while producing exactly the same results. The effect of distance between the human head and the antenna on the SAR and the temperature rise is also investigated. The maximum 1 gram SAR and temperature rise at 900 MHz and 1.5 GHz are given in Table 3 when the distance between the human head and the antenna is changed.

Table 3: Distance effect on SAR and temperature rise

Distance	Max. Temp. Rise [°C]		Max. SAR_{1g} [Watt/kg]	
	900 MHz	1.5 GHz	900 MHz	1.5 GHz
28 mm	0.239	0.120	1.364	0.851
36 mm	0.174	0.080	0.965	0.568
44 mm	0.129	0.058	0.698	0.407

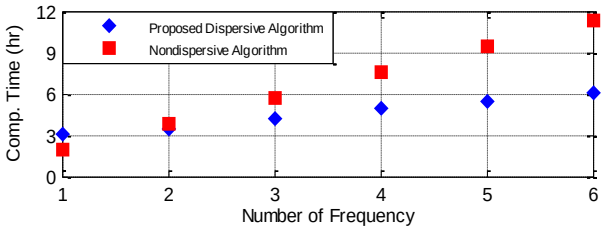

Fig. 8. Comparison of the computation time performed by both algorithms vs. number of frequency.

IV. CONCLUSION

An efficient algorithm is developed for the computation of the temperature rise and SAR distributions in a head model due to the radiation from a nearby antenna operating at 900 MHz and 1.5 GHz. The maximum temperature rise is 0.281 °C at 900 MHz and 0.149 °C at 1.5 GHz with antenna output powers of 0.6 W at 900 MHz and 0.27 W at 1.5 GHz, respectively. The key contribution here is the computation of the temperature rise and SAR distributions at multiple frequencies in a single FDTD simulation. Remarkable saving in computation time is achieved when the analysis is performed at more than one frequency.

REFERENCES

[1] J. Wang and O. Fujiwara, "FDTD computation of temperature rise in the human head for portable

telephones," *IEEE Trans. Microwave Theory Tech.*, vol. 47, pp. 1528-1534, Aug. 1999.

[2] P. Bernardi, M. Cavagnaro, S. Pisa, and E. Piuzzi, "Specific absorption rate and temperature increases in the head of a cellular-phone user," *IEEE Trans. Microwave Theory Tech.*, vol. 48, pp. 1118-1126, July 2000.

[3] P. Bernardi, M. Cavagnaro, S. Pisa, and E. Piuzzi, "Power absorption and temperature elevations induced in the human head by a dual-band monopole-helix antenna phone," *IEEE Trans. Microwave Theory Tech.*, vol. 49, no. 12, pp. 2539-2546, Dec. 2001.

[4] A. Hirata, M. Morita, and T. Shiozawa, "Temperature increase in the human head due to a dipole antenna at microwave frequencies," *IEEE Trans. Electromag. Compat*., vol. 45, no. 1, pp. 109-116, Feb. 2003.

[5] A. Hirata, and T. Shiozawa, "Correlation of maximum temperature increase and peak SAR in the human head due to handset antennas," *IEEE Trans. Microw. Theory Tech*., vol. 51, no. 7, pp. 1834-1841, July 2003.

[6] M. Fujimoto, A. Hirata, J. Q. Wang, O. Fujiwara, and T. Shiozawa, "FDTD-derived correlation of maximum temperature increase and peak SAR in child and adult head models due to dipole antenna," *IEEE Trans. Electromagn. Compat.*, vol. 48, no. 1, pp. 240-247, Feb. 2006.

[7] A. Hirata, K. Shirai, and O. Fujiwara, "On averaging mass of SAR correlating with temperature elevation due to a dipole antenna," *Progress In Electromagnetics Research*, vol. 84, pp. 221-237, 2008.

[8] M. R. Islam and M. Ali, "Temperature rise induced by wire and planar antennas in a high-resolution human head model," *IEEE Trans. Electromagn. Compat*., vol. 55, no. 2, pp. 288-298, Apr. 2013.

[9] A. Z. Elsherbeni and V. Demir, *The Finite-Difference Time-Domain Method for Electromagnetics with MATLAB Simulations*. second edition, ACES Series on Computational Electromagnetics and Engineering, SciTech Publishing, an Imprint of IET, Edison, NJ, 2016.

[10] H. H. Pennes, "Analysis of tissue and arterial blood temperature in resting forearm," *J. Appl. Physiol*., vol. 1, pp. 93-122, 1948.

[11] M. A. Eleiwa and A. Z. Elsherbeni, "Debye constants for biological tissues from 30 Hz to 20 GHz," *ACES Journal*, vol. 16, no. 3, Nov. 2001.

[12] http://noodle.med.yale.edu/zubal/ [Online website 2017].

[13] S. Gabriel, R. W. Lau, and C. Gabriel, "The dielectric properties of biological tissues: III. Parametric models for the dielectric spectrum of tissues," *Phys. Med. Biol*., 41, pp. 2271-2293, 1996.

[14] J. Roden and S. Gedney, ''Convolution PML (CPML): An efficient FDTD implementation of the CFS-PML for arbitrary media," *Microwave and Optical Technology Letters*, vol. 27, no. 5, pp. 334-339, 2000.

[15] *IEEE Recommended Practice for Measurements and Computations of Radio Frequency Electromagnetic Fields With Respect to Human Exposure to Such Fields, 100 kHz-300 GHz*, IEEE Standard C95.3-2002, Annex E, 2002.

Fatih Kaburcuk received both the M.Sc. and Ph.D. degrees from Syracuse University, Syracuse, New York in 2011 and 2014, respectively, all in Electrical Engineering. Kaburcuk is an Assistant Professor at Erzurum Technical University, Turkey.

Atef Z. Elsherbeni received his Ph.D. degree in Electrical Engineering from Manitoba University, Winnipeg, Manitoba, Canada, in 1987. Elsherbeni was with the University of Mississippi from 1987 to 2013. He was a Finland Distinguished Professor from 2009 to 2011. He joined the Electrical Engineering and Computer Science Department at Colorado School of Mines in August 2013 as the Dobelman Distinguished Chair Professor. Currently he is the Head of the Electrical Engineering Department. His research interest includes the scattering and diffraction of EM waves, finite-difference time-domain analysis of antennas and microwave devices, field visualization and software development for EM education, interactions of electromagnetic waves with the human body, RFID and sensor integrated FRID systems, reflector and printed antennas and antenna arrays, and measurement of antenna characteristics and material properties. His academic achievements include: Funded Research Grants with a total amount of $11,413,903, 13 books, 29 book chapters, 171 journal publications, 15 developed software packages, 56 (35 MS and 21 PhD) graduate students advised, 40 invited presentations, 221 proceedings publications, 174 conference abstracts, 74 technical reports, 35 short courses offered, 43 invited talks. Elsherbeni is a Fellow Member of IEEE and ACES. He is the Editor-in-Chief for ACES Journal. He was the general Chair for the 2014 APS-URSI Symposium and was the president of ACES Society from 2013 to 2015.